Macromolecules

Article

Cite This: Macromolecules XXXX, XXX, XXX−XXX

Sensitivity of Polymer Crystallization to Shear at Low and High Supercooling of the Melt

Alicyn M. Rhoades,*[,†] Anne M. Gohn,[†,‡] Jiho Seo,[§] René Androsch,[‡] and Ralph H. Colby[§]

[†]Pennsylvania State University, Behrend College, 4701 College Drive, Erie, Pennsylvania 16563, United States

[‡]Interdisciplinary Center for Transfer-oriented Research in Natural Sciences, Martin Luther University Halle-Wittenberg, 06009 Halle/Saale, Germany

[§]Department of Materials Science and Engineering, Penn State University, University Park, Pennsylvania 16802, United States

ABSTRACT: Flow-induced crystallization (FIC) is a dominant mechanism of polymer self-assembly, but the process is poorly understood at high supercooling and under fast cooling conditions because of structural rearrangements that occur during slow heating and cooling conditions typically used for investigation. Incorporating fast-scanning chip calorimetry techniques, the influence that specific amounts of shear flow have on the subsequent crystallization of polyamide 66 over a wide range of temperatures, 85−240 °C, is determined. At high temperatures, heterogeneous nucleation dominates and crystallization rate increases with increasing shear. Low-temperature crystallization, driven by homogeneous nucleation, is not influenced by previous shear flow, but sheared samples are able to crystallize via the heterogeneous nucleation route at temperatures 15 K lower than unsheared materials. The magnitude of previous shear flow also dictates α-/γ-crystalline phase development and crystallization during cooling at rates below 200 K/s. This approach provides a route to develop important thermodynamic and kinetic insights that describe the crystallization behavior of many important polymers to enable the advanced engineering of polymer processing and injection molding applications, where practical cooling rates typically range between 10 K/s and 1000 K/s.

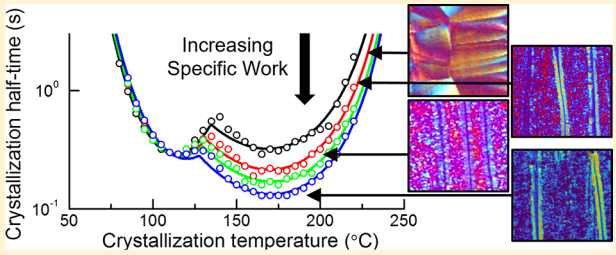

1. INTRODUCTION

Flow-induced crystallization (FIC) is a linchpin phenomenon that, when understood, has the potential to unlock major advances in polymer engineering. Despite many research gains in FIC during the past 30 years, practical implementation of the findings is rare because the results do not access crystallization behaviors such as those that occur during polymer manufacturing processes such as injection molding.[1−4] Understanding these crystallization behaviors, which occur after the polymer melt is subject to strong flow, rapid cooling, and high supercooling, is required if engineers are expected to evolve key aspects of polymer processing from more of an "art" to a truly applied science.[5−8]

In the past decade, a renaissance has taken place in the field of *unsheared*, quiescent polymer crystallization as researchers have established crystallization behaviors for many polymers across temperatures spanning from the glass transition temperature (T_g) to the equilibrium melting temperature (T_m^0), at high melt supercooling, and under high heating and cooling rates.[9] These advances are largely due to the introduction of fast scanning chip calorimetry (FSC) techniques that can induce fast thermal cycling while sensing thermal transitions in nanogram-size polymer samples, minimizing the thermal lag that limits standard thermal analysis. Typical heating and cooling rates employed for polymers exceed 1000 K/s, allowing investigations of isothermal crystallization at temperatures near T_g without any crystallization occurring as the polymer is rapidly cooled from the melt.[9−11]

Many flexible polymers display qualitatively similar isothermal crystallization behavior between T_g and a temperature approximately 5 K below the melting temperature (T_m) of a slowly cooled sample.[10] During slow cooling, polymers typically crystallize at relatively high temperatures (low supercooling) via a heterogeneous nucleation mechanism. Nucleating agent additives are predicated on this mechanism; increasing heterogeneous nucleating sites will increase the rate of polymer crystallization during cooling.[12,13] Decreasing the temperature (increasing supercooling) causes an increase in crystallization rate until a specific temperature that facilitates the fastest rate. Further cooling causes crystallization rates to decrease due to slower polymer diffusion to growing sites. However, examining the halftime of isothermal crystallization for many polymers at discrete temperatures across the entire temperature range consistently reveals that the crystallization nucleation rate will again increase at even higher supercooling, before slowing down again at crystallization temperatures that approach T_g. Likely, this common bimodal crystallization rate vs temperature

Received: January 26, 2018
Revised: March 20, 2018

DOI: 10.1021/acs.macromol.8b00195
Macromolecules XXXX, XXX, XXX−XXX

relationship is due to a change in the dominant mechanism of polymer crystallization from heterogeneous nucleation at low supercooling to homogeneous nucleation at high supercooling.[14] While heterogeneous nucleation sites are still present in the polymer at high supercooling, the sheer number of homogeneous nucleation sites results in a solidification process dominated by homogeneous nucleation. Because the homogeneous nucleation density is so high, the resulting solid polymer typically does not display spherulitic structure, and the ordered domains are very small (<10 nm) and are not visible by polarized light. Such behavior seems typical for all polymers and has been evidenced by experiments for polyamide 66 (PA 66), polyamide 6 (PA 6), isotactic polypropylene (iPP), poly(butylene terephthalate) (PBT), polyamide 11 (PA 11), and several random copolymers of propylene with 1-alkenes despite obvious differences in chain architecture.[11,15−17] Some polymers, such as poly(ε-caprolactone) (PCL), poly(ethylene terephthalate) (PET), and poly(L-lactic acid) (PLLA), do not display a clear low-temperature minima. However, experimental evidence proves these polymers also undergo homogeneous nucleation at low temperatures, and so the behavior appears to be ubiquitous.[13,18,19]

Polymers crystallized from a sheared melt display (a) greatly increased number density of crystal nuclei, (b) accelerated crystallization after shearing, (c) anisotropic solidified morphology due to aligned nuclei, and (d) an increased lifetime of nuclei, all with respect to the quiescent equivalent.[20] While the FIC process still holds innumerable questions, major steps are confirmed. The longest chains in the melt have the longest characteristic relaxation times and are therefore affected first under a given flow field. If the shear rate exceeds the reciprocal of the Rouse time ($1/\tau_R$), then chain extension occurs.[21] Under a flow field in the melt, the polymer chains align and stretch. This extended chain state results in a semiordered, mesomorphic structure with an aspect ratio of up to 10 000 in the fully extended state, defined herein by the term *flow-induced precursor* for crystal nucleation.[22] These precursors have both additional thermodynamic and kinetic motivation to crystallize. Thermodynamically, the entropy of this extended conformation is lower than random-walk coils. The mesomorphic structure is closer to the crystal form than the liquid state, so there is a lower free energy barrier to overcome in crystallization.[23] These favorable attributes cause crystallization of the threadlike precursor to happen first, forming the *shish* chain-extended crystal. The shish then acts as a nucleating surface for surrounding coiled chains, which crystallize into folded-chain lamellae (*kebabs*) that grow perpendicular to the shish surface.[24−29]

The formation of nucleating shish crystals and the lateral growth of kebabs occur in two distinct stages, separated in time by the cessation of flow. Recent experiments have confirmed that for isotactic polypropylene the nucleation step and growth of a small amount of chain-extended crystals, which comprise about 7% of the total growth, occur during flow while the majority of chain-folded lamella (kebab and spherulite) growth occurs after the cessation of flow.[30,31] We use this fact to our advantage as we first shear to create shish-kebab structures and then remelt and recrystallize the kebab fraction of our samples in the calorimetric studies.

In this study, PA 66 was chosen to study the change in crystallization due to shear work in both the heterogeneous, low supercooling and homogeneous, high supercooling range. For this investigation, molten PA 66 is carefully subject to known amounts of shear and then solidified. After solidification, the sample is removed from the rheometer and sectioned for subsequent crystallization studies using FSC. Capitalizing on this stability of FIC nuclei at temperatures lower than T_m^0, a single sample can be sufficient to evaluate repeatedly under all temperatures and rates of interest, with crystallization taking its genesis from the flow-induced precursors.[32−35] Thanks to the thermal stability of the precursors, flow-induced nucleation density remains constant between the many thermal studies carried out for a given sheared sample. Using this approach, the influence that these flow-induced crystal precursors exert in the melt on subsequent crystallization is quantified across the entire possible crystallization temperature range, both isothermally and during a range of cooling rates such as those the polymer melt may encounter during processing.

While several variables contribute to FIC, a single working term combines the effects of shearing time (t_s), shearing rate ($\dot{\gamma}$), and temperature of the melt during shear (T_s) into "specific work" (W). During flow, the deformations caused by W drive the FIC process.[36−41] The equation for specific work (W) is shown in eq 1, where σ is the applied stress and η the shear viscosity at the applied shear rate ($\dot{\gamma}$).

$$W = \sigma\gamma = \eta\dot{\gamma}^2 t_s \tag{1}$$

At low levels of W, there is no influence on ensuing crystallization processes. However, there are defined flow regimes that result from increasing the amount of specific work W in the melt, as evidenced by changes in the solidified polymer microstructure.[42] A critical amount of work (W_c) is required to induce oriented structures.[1,40,43,44] In this study, we intentionally exceed the W_c to create oriented PA 66 with known levels of W using a parallel plate rheometer.[39]

For engineering considerations, the leap must be made to investigate FIC behaviors at high supercooling of the melt.[8] While experimental evidence suggests that FIC is dependent on both the degree of supercooling and the previous rate of shearing at high temperatures, rate constants and crystallization behaviors at high supercooling are currently estimated by extrapolating the crystallization rate constant obtained at low-supercooling conditions to high supercooling of the melt.[2] The concept that flow-induced precursors and chain-extended shish formed during FIC are active in subsequent crystallization mechanisms even after a quench/remelting cycle, provided the temperature does not exceed T_m^0, is essential to the design of our study. Because of this stability, the accelerating influence of these structures should be observable at high supercooling using FSC techniques.

2. EXPERIMENTAL SECTION

2.1. Materials. The PA 66 material used in this study was commercial Zytel 101, from DuPont (USA). It is an unlubricated and unmodified general-purpose molding-viscosity grade, selected for this study to ensure that no additives are present that may influence (nucleate or hinder) the crystallization process. The material was available in pellet form and was dried for 20 h at 80 °C before use according to manufacturer specifications.[45] Kapton tape used for the fabrication of discs was purchased from Makerbot (USA). The molecular weight (M_w = 22 700 g/mol, M_n = 11 300), molecular weight distribution, and calculated longest chain length were determined using size exclusion chromatography. The zero-heating-rate glass transition temperature (T_g) is reported to be 60 °C using standard DSC techniques. The equilibrium melting temperature and bulk heat of fusion of the α-phase are 277.4 °C (547 K) and 255 J/g,

DOI: 10.1021/acs.macromol.8b00195
Macromolecules XXXX, XXX, XXX−XXX

respectively. The equilibrium melting temperature was experimentally determined using the linear Hoffman–Weeks approach.[46]

2.2. Size Exclusion Chromatography (SEC). SEC (LC-20AD, Shimadzu, Japan) was used to measure the molecular weight and molecular weight distribution. Two analysis columns (HFIP-606M, Shodex, Japan), one guard column (HFIP-G, Shodex, Japan), and a differential refractive index detector (RI-104, Shodex, Japan) were used with a mobile phase of 1,1,1,3,3,3-hexafluoro-2-propanol (HFIP, CAS# 920-66-1) containing 5 mM sodium trifluoroacetate (NaTFA, CAS# 2923-18-4). A 20 mL injection volume was used, and the flow rate was 0.2 mL/min at 40 °C. First, 100 mg of PA 66 was dissolved in 1 mL of HFIP/NaTFA solution, stirred overnight, and diluted to the concentration of 0.05 wt %. The prepared solution was then filtered before injection using a Millex syringe filter (EMD Millipore, Billerica, MA) with 0.45 μm pore. The molecular weight and molecular weight distribution curve were determined, relative to poly(methyl methacrylate) (PMMA) standards. The molar mass of PA66 was then calculated using the reported Mark–Houwink parameters; $K_{PMMA} = 0.115 \times 10^{-3}$, $a_{PMMA} = 0.746$, $K_{Nylon6/6} = 1.236 \times 10^{-3}$, and $a_{Nylon6/6} = 0.673$.[47] $M_w = 22\,700$ g/mol, $M_n = 11\,300$.

2.3. Polarized-Light Optical Microscopy (POM). Samples were imaged using POM employing a Leica DM750P microscope and DMC2900 camera. Prior to FSC analysis, the microtomed cross sections of the disc were inspected for flow-induced structures. Careful cutting of the samples under POM allowed for the selection of samples with known shish-kebab content. Between FSC analyses, the sensor containing the sample was moved to the microscope for microstructure evaluation.

2.4. X-ray Diffraction (XRD). Wide-angle X-ray scattering (WAXS) experiments were performed directly on samples mounted in the Mettler-Toledo MultiSTAR flash DSC sensor under vacuum using a SAXS/WAXS laboratory system (Xeuss 2.0 HR, Xenocs, France) using a microfocus sealed X-ray tube (Cu 1.54 Å) operated at 50 kV and 0.6 mA as the source. The system is equipped with a Pilatus3 R200K detector, and the sample-to-detector distance was approximately 0.15 m. The scattering experiments were collected at room temperature, and the 2D images were integrated over a tilted circle profile to convert to one-dimensional scattering data of scattering intensity $I(q)$ (in arbitrary units) versus 2θ. The resulting data were denoised by wavelets using Jade 2010 software (Materials Data, Inc., Livermore, CA).

2.5. Sample Preparation. To probe the role of shear-induced structures on subsequent crystallization, three PA 66 sample discs were fabricated using a rotational rheometer. The discs were sheared to intentionally develop a series of known maximum specific work W at the outer radii (9, 73, and 290 MPa). The shearing time was the only variable during fabrication; all other variables were kept constant between the sample discs. Any differences in the resulting microstructure are due to this time-sensitive aspect of FIC development, and such samples are routinely characterized using POM.[39] Fabrication employed an ARES-G2 rheometer (TA Instruments, New Castle, DE) equipped with 25 mm stainless steel parallel plate fixtures. Before loading the PA 66 pellets on the parallel plate, Kapton tape was attached on both top and bottom plates to facilitate easy removal of the sheared disc after solidification for subsequent microscopic and calorimetric analysis. The geometry held 1.2 mm gap during the entire fabrication. Parallel plate measurements were used to confirm that the Kapton tape introduced no variation to the shear flow of the polymer during the sample preparation.

A time–temperature protocol that employed both rotational and oscillatory shear was developed for the sheared-disc fabrication. First, PA 66 pellets, after being dried at 80 °C in a vacuum oven overnight, were melted on parallel plate fixtures at 270 °C for 1 min. A constant shear rate of ~0.5 s^{-1} was then applied to the molten pellets for ~5 min to aggregate the pellets without air bubbles. To erase the thermal history, the temperature of the polymer melt was increased to 300 °C for 1 min. After this annealing step, the melt was cooled (10 K/min) to the shearing temperature of 270 °C, and a designated shear rate at the perimeter (100 s^{-1}) and shearing time (0.81, 6.5, and 25.9 s for the three different discs) were imposed on the melt to achieve three specific works of interest. After shearing, the melt was cooled at 10 K/min to 200 °C and held for 5 min, which is sufficient time to ensure complete crystallization. The sample was then cooled (10 K/min) to room temperature, and the solidified discs were removed from the parallel plate fixture for ongoing studies. A fourth "zero shear" sample was prepared using an identical protocol, but instead of shearing at 270 °C the material was simply held in the melt for 25.9 s at 270 °C and then solidified under conditions identical to the corresponding sheared samples.

For each disc prepared, there is a distribution of the shear rate and specific work across the radius of the parallel plate disc as shown in Figure 1. The shear rate is determined by the velocity of the rotation

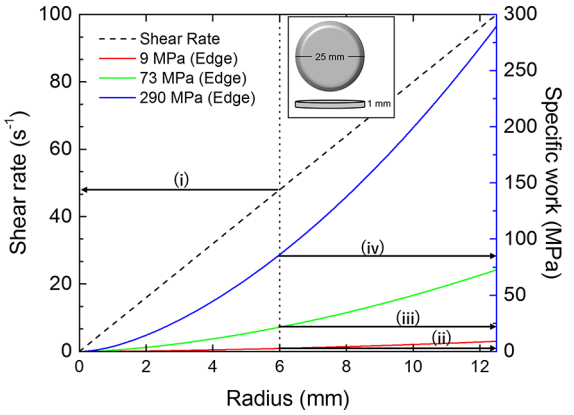

Figure 1. Shear rate and resulting specific work as a function of disc radius are plotted for each sample. (i) Each of the four discs experienced a shear rate of 48 s^{-1} at a 6 mm distance from the center as indicated. The specific work developed across the disc radii is plotted, and the specific work level developed at the 6 mm disc position is indicated by arrows. Arrow (ii) indicates specific work of 3 MPa, arrow (iii) indicates specific work of 22 MPa, and arrow (iv) indicates a specific work of 86 MPa acted upon the polymer at the 6 mm sampling location. The inset box depicts the disc geometry prepared in the rotational rheometer.

and the distance between the plates, resulting in a linear increase in shear rate from the radius to the edge. Theoretically, the shear rate at the center of the disc is zero. However, POM of this center location consistently reveals a small bit of orientation influencing material solidification, perhaps due to a drag force present in the melt, likely modifying the crystallization process relative to a truly unsheared sample. The specific work for each of the three discs used in this study is plotted in Figure 1 as a function of radius from the center of the disc, spanning the cross section. The specific work depends on the shear stress per eq 1, using a steady-state shear viscosity measurement of 1400 Pa·s obtained via cone and plate rheology measurements.

The solidified discs were sectioned radially and subsequently microtomed perpendicular to the direction of flow to obtain sections with a thickness of 12 μm. From each disc, a sampling location of 6 mm from the zero-shear position of the microtomed strip was chosen, indicated in Figure 1 by arrows (ii, iii, and iv). At this location in each disc, the material that had experienced a shear rate of 48 s^{-1} indicated by arrow labeled (i) and the local specific work was 3 MPa (ii), 22 MPa (iii), and 86 MPa (iv). At the 6 mm location on the microtomed strip, specific shish-kebab structures are easily visible, and several were selected for thermal analysis.

2.6. Isolating FIC Structures for FSC Characterization. For this study, 12 μm thick samples were microtomed and then laterally cut (75 μm × 75 μm) from each disc of the three sheared discs at the 6 mm radial position, resulting in samples containing 3, 22, and 86 MPa of W, respectively. An identical sample was taken from a disc fabricated with $W = 0$ MPa, referred to as the unsheared disc. Figure 2 clearly show shish-kebab structures that are visible in the microtomed strips from each sample disc. The unsheared disc does not display shish-

DOI: 10.1021/acs.macromol.8b00195
Macromolecules XXXX, XXX, XXX–XXX

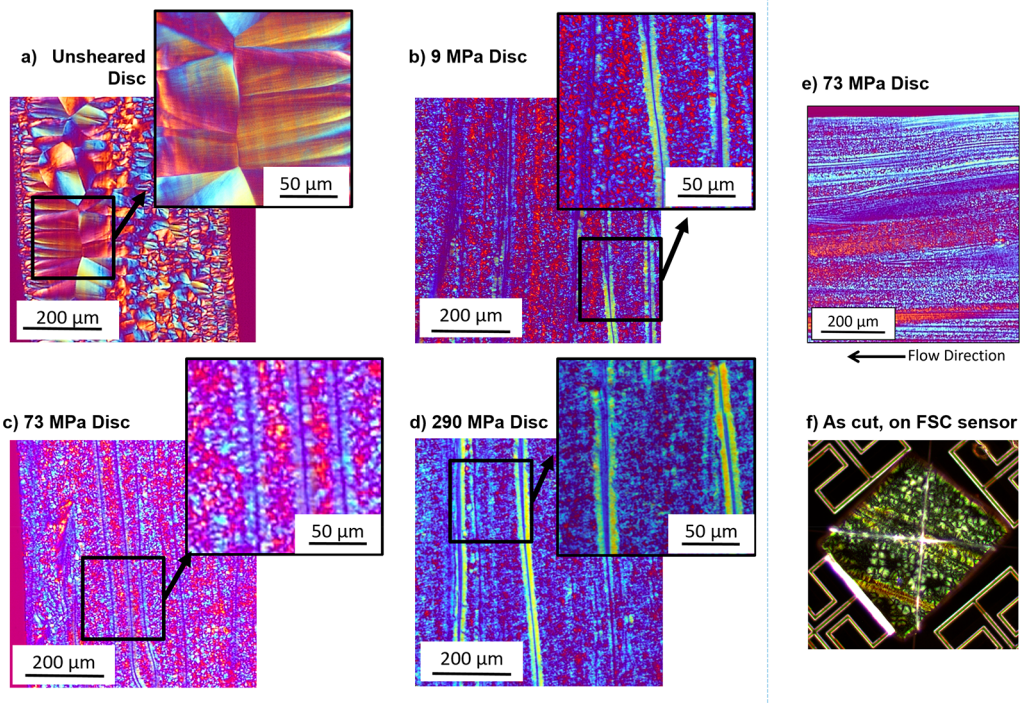

Figure 2. Polarized-light microscopy images of sheared samples for FSC analysis: (a) unsheared (0 MPa) disc at 6 mm location, (b) 9 MPa disc at 6 mm location (W = 3 MPa), (c) 73 MPa disc at 6 mm location (W = 22 MPa), and (d) 290 MPa disc at 6 mm location (W = 86 MPa). All subset boxes indicate typical areas selected for FSC analysis. Flow direction is perpendicular to the surface shown for (b–d). (e) Shish-kebab structures from the same sample represented in (c), grown in the direction of flow. (f) Example of a sample extracted from the 6 mm position and placed on the FSC sensor for calorimetric analysis. For all sheared samples $\dot{\gamma}$ is 48 s^{-1} at the location of FSC sampling.

kebab structures, but large spheurilites can be easily observed as in Figure 2a.

While many shish-kebab structures were visible in the direction of flow as shown in Figure 2e, the largest shish-kebab structures selected for further analysis were solidified perpendicular to the flow and are easily visible in each cut sample under POM. Shish oriented perpendicular to the shearing direction is analogous to the "log-rolling" orientation of some fraction of the chains seen in thermotropic liquid crystalline polymer systems in shear flows.[48,49] Considering the rigidity of chain-extended crystalline structures that comprise shish, it is not surprising to find similar development of orientation in the flow-induced melt crystallization of flexible polymers.[50] The shish must form in the direction of shear, but small perturbations in flow can introduce a reversible orientation transition 90° from the flow direction to the vorticity direction, referred to as "log-rolling alignment".[51] For each FSC study, a sample area of 75 μm × 75 μm, containing shish-kebab structures visible in polarized light, was cut out of the 12 μm thick film. This small square of polymer film was transferred to the heatable area of the FSC sensor chip, and the polymer microstructure was visible on the FSC chip prior to calorimetric studies. The shish-kebabs were intermittently observed using POM to aid in our interpretation of the calorimetric studies.

2.7. Fast Scanning Calorimetry (FSC). FSC analysis was performed using a power-compensation Mettler-Toledo Flash DSC 1, attached to a Huber intracooler TC100. Prior positioning of the specimen on the heatable area of the sample calorimeter, the UFS 1 FSC sensor was conditioned and temperature-corrected according to the specification of the instrument provider. The calorimeter was purged with dry nitrogen gas at a flow rate of 35 mL/min. The sample mass was between 120 and 300 ng and was estimated by comparing the measured heat-capacity increment on heating a fully amorphous sample at the glass transition temperature T_g in units of J/K with the expected mass-specific heat-capacity increment of 0.51 J /(g K).[41] Further details about the instrument/sensor are reported in the literature.[52−54] To select samples for FSC measurements, the molded specimens were cut perpendicular to the flow direction to obtain sections with a thickness of 12 μm using a rotary microtome equipped with a tungsten carbide blade. The samples were quenched using liquid nitrogen prior to cutting to prevent ductile failure from the blade. A similar sampling approach was developed to observe the relaxation of FIC precursors in poly(lactic acid) using fast calorimetric techniques, but crystallization behaviors were not observed.[55] Prior to placing the sample on the FSC chip, a thin layer of thermally stable silicone fluid (Wacker AK 60000) was applied to the surface of the chip to aid in heat transfer and to prohibit the sample from fusing to the chip.

2.7.1. Isothermal Crystallization. The FSC protocol to analyze the isothermal crystallization behavior of PA 66 was similar to the protocol used in previous work, except that the maximum temperature of the melt chosen in this work, typically 275 °C, is lower than the equilibrium melting temperature of 277.4 °C determined for this grade of PA 66.[56] The method is depicted in Figure 3a. The lower maximum temperature ensures that FIC nuclei formed during the shearing process were not destroyed in the melt but were preserved through the series of calorimetric studies. The samples cut from the microtomed discs were placed onto a FSC sensor chip and then subject to a temperature profile that first melted the PA 66 at 275 °C, followed by a rapid (2000 K/s) quench to the isothermal crystallization temperature of interest. After isothermal crystallization was complete, the sample was quenched to −60 °C and then heated at a rate of 1000 K/s to 275 °C, melting the sample in preparation for the next target isothermal crystallization temperature in the series. The process was repeated until each isothermal temperature was complete. The half-time of crystallization, defined as the time when 50% of the crystallization is complete, is experimentally determined from the crystallization isotherm.

2.7.2. Nonisothermal Crystallization. FSC analysis was then employed to study the nonisothermal crystallization behavior of PA 66 at differing specific work conditions. In this thermal analysis method, the sample was heated at a rate of 1000 K/s from 25 to 275 °C and held in the melt at this temperature for 0.5 s, again remaining below the equilibrium melting temperature to preserve any flow-

DOI: 10.1021/acs.macromol.8b00195
Macromolecules XXXX, XXX, XXX−XXX

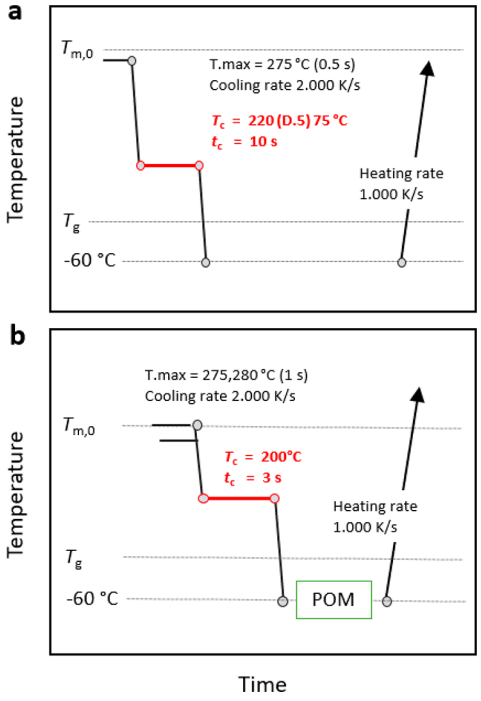

Figure 3. Methods for FSC analysis: (a) isothermal crystallization; (b) nuclei survival studies executed on the FSC.

induced structures. The polymer sample was then cooled at a specific rate between 1 and 5000 K/s to −60 °C where it was held for 0.5 s. A subsequent heating rate of 500 K/s was used to analyze the crystallinity that was formed during cooling. Once back at the maximum temperature of 275 °C, the PA 66 sample was conditioned at the next cooling rate in the sequence. This process was repeated until all cooling rates were analyzed. The enthalpy of any cold crystallization on heating was subtracted from the melting enthalpy to obtain an enthalpy value that represents the crystallinity formed on cooling. This enthalpy value was then converted to a percent crystallinity based on the sample size.

2.7.3. Nuclei Survival Method. The sheared samples tested in the FSC for the nuclei survival evaluation were analyzed using the same sample, repeatedly, according to the method shown in Figure 3b. In order to confirm that the nucleating characteristic of the shish was not deteriorating in the melt between isothermal steps, the experiment was duplicated with the same sample and isotherms from each series of experiments were identical. To establish the rate of shish disassociation or relaxation in the melt, a survival experiment was designed to determine the onset time of disassociation, evidenced by slower isothermal crystallization. To establish the amount of time that shish survive at specific temperatures, samples containing shish from the 22 MPa location of the 73 MPa disc were selected. In this experiment, the sample was first taken to 275 °C for 0.2 s, quenched at 2000 K/s to 200 °C, and allowed to isothermally crystallize for 3 s. 200 °C was chosen for the crystallization temperature, as it has previously been proven to produce spherulitic structures in this system.[56] After crystallization was complete, the sample was quenched at 2000 K/s to room temperature and imaged using POM. After imaging, the same sample was placed back into the FSC and heated to the target maximum temperature, where it was held for 1 s, and quenched at 2000 K/s to crystallize at 200 °C prior to POM imaging. The thermal trace of the isothermal crystallization along with the resulting POM images allowed for calorimetric and kinetic evaluation of the shish stability at 275 °C (below T_m^0) and 280 °C (above T_m^0). New samples were prepared for each temperature of interest.

3. RESULTS AND DISCUSSION

This study aims to determine the sensitivity of crystallization behavior to the exact amount of specific work imparted to the material prior to solidification across the relevant temperature spectrum and during a series of cooling rates. Because the sample size for FSC is sufficiently small (approximately 75 ng), it is possible to isolate shish-kebab structures created under very exact, known conditions and then quantify their influence on subsequent crystallization processes. The concept that the flow-induced precursors can survive temperatures in the melt up to but not exceeding T_m^0 remains central to this study. Each of the following studies will confirm that the flow-induced acceleration of crystallization repeatedly occurs as a single sample is melted, undergoes crystallization and solidification, and is again melted for subsequent studies. In the final section we discuss how these flow-induced effects diminish with increasing time at $T > T_m^0$.

3.1. Isothermal Crystallization. The isothermal crystallization half-time data detailed in Figure 4a represent the first unambiguous, quantitative evidence that flow-induced nuclei precursors formed during a shear step survive to nucleate subsequent crystallization events at moderate supercooling, but they do not dominate crystallization at high supercooling. In this experiment the flow-induced precursors and the visible shish structures, formed during shearing in the rotational rheometer, were present for subsequent isothermal crystallization studies in the FSC because the temperature of the melt was limited to 275 °C, which is below the equilibrium melting temperature.

At isothermal crystallization temperatures higher than 135 °C the accelerating effects of flow-induced nucleation, the magnitude of which parallel the amount of work (W) to which each sample was subject, are obvious. With increasing work experienced by the PA 66 there is a systematic decrease in crystallization half-time relative to the unsheared sample even at relatively high supercooling (ΔT_s = 145 K at a crystallization temperature of 135 °C). These reduced peak times occur across the range of temperatures known to facilitate heterogeneous nucleation, between 135 and 230 °C. The mechanism is clearly optimized at the isothermal temperature of about 170 °C, where crystallization occurs at the highest rate. The flow-induced structures in the melt act to nucleate in a fashion reminiscent of systems containing purposely added heterogeneous nucleating agents or those containing nanofillers.[57−60]

In the low-temperature range (T_c < 135 °C), crystallization is dominated by a homogeneous nucleation mechanism, supported by the lack of any accelerated crystallization of our sheared samples in this temperature range. Several researchers have shown that heterogeneities only control crystallization at lower supercooling, despite being present in the matrix at all temperatures.[59,61] At low temperatures and high supercooling, the concentration of flow-induced precursors is likely too low to compete with homogeneous nuclei.[16] The heterogeneous crystallization process is limited by chain diffusion to nucleation sites; therefore, homogeneous nucleation dominates, and the presence of shish or threadlike precursors logically does not influence this process. The half-time of crystallization of all sheared samples converges with the nonsheared sample at a crystallization temperature of about 110 °C; this low-temperature peak-time minimum is likely due to the onset of the formation of homogeneously nucleated domain-like γ-mesophase. Previous studies of the PA 66 have established 110 °C as

DOI: 10.1021/acs.macromol.8b00195
Macromolecules XXXX, XXX, XXX−XXX

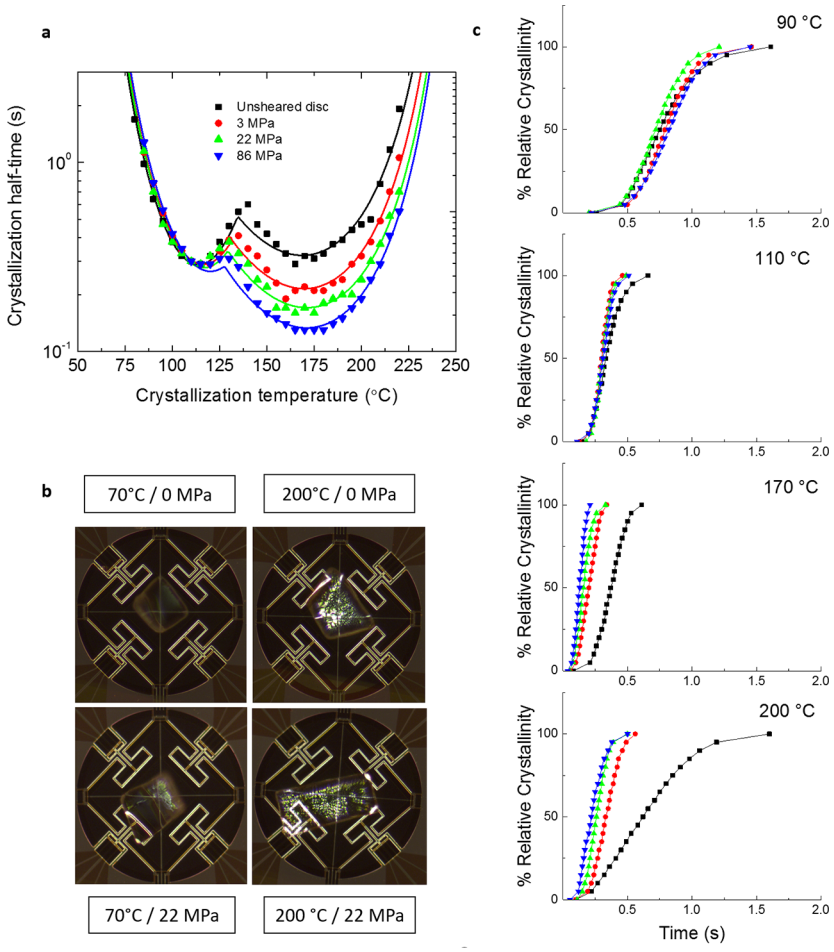

Figure 4. Isothermal crystallization. (a) Half-time of crystallization for each PA 66 sample at each temperature studied. (b) POM images depicting the resulting crystallinity formed upon isothermal crystallization at the indicated temperature on the FSC sample chip. The black circle containing the sample is the heated area of the FSC sensor chip and has a diameter of 500 μm. At 70 °C, the lack of birefringence is characteristic of the γ-mesophase. At 200 °C, visible birefringence indicates α-phase structure.[56] (c) Percent crystalline conversion as a function of time for PA 66 samples in the heterogeneous nucleation range (200 and 170 °C), at the homogeneously nucleated, low-temperature minimum (110 °C) and squarely in the homogeneous nucleation range (90 °C). Colors are defined in the Legend of part (a).

the transition temperature, above which spherulitic α-crystallization occurs and below which there is the fast formation of the mesophase.[56] Indeed, microfocused wide-angle X-ray analysis confirmed that the 22 MPa sample, isothermally crystallized at 70 °C, also primarily formed the γ-mesophase, while isothermal crystallization at 200 °C formed the stable α-phase.

Figure 4b shows POM micrographs of sheared and unsheared PA 66, isothermally crystallized at 70 and 200 °C as indicated, with sample preparation taking place in the FSC. After the isothermal crystallization step, the samples were quenched (−1000 K/s) to 25 °C to prohibit any structural changes and then examined using both POM and microfocus wide-angle X-ray diffraction (XRD). The POM images illustrate that there is a qualitative difference in the transparency/birefringence of the samples crystallized in the homogeneous, low-temperature range relative to the high-temperature, heterogeneous nucleation range. In the samples crystallized at 200 °C, there is a higher nucleation density observable in the sample previously subject to shear. XRD analysis reveals identical structures that had ultimately developed at 70 °C (γ-mesophase) and 200 °C (α-phase) for sheared and nonsheared samples. However, the rate at which each of these micro-structures formed reveals much about the process of crystallization within the two temperature regimes. Figure 4c details the development of crystallinity with time for each sample at four different temperatures of interest. At all temperatures detailed, the no-shear sample requires more time to complete crystallization. In the heterogeneous nucleation regime (170 and 200 °C) the onset of crystallization also requires more time for the no-shear sample, while the onset of crystallization—driven by nucleation—decreases with increasing exposure to shear work. In the low temperature range (70 and 110 °C) the onset of crystallization is not influenced by any shear precursors present, though the conversion process requires more time to reach completion at 110 °C relative to the sheared counterparts.

Other insights from this straightforward isothermal crystallization behavior are noteworthy. At the levels of specific work studied, the acceleration of crystallization in the high-temperature regime did not saturate, indicating that further acceleration may be possible if the PA 66 melt is subject to a higher amount of work. Second, one can observe a 15 K shift in the temperature at which the polymer transitions from the high-temperature process to the low-temperature process with increasing shear work. For the no-shear sample, the transition

DOI: 10.1021/acs.macromol.8b00195
Macromolecules XXXX, XXX, XXX−XXX

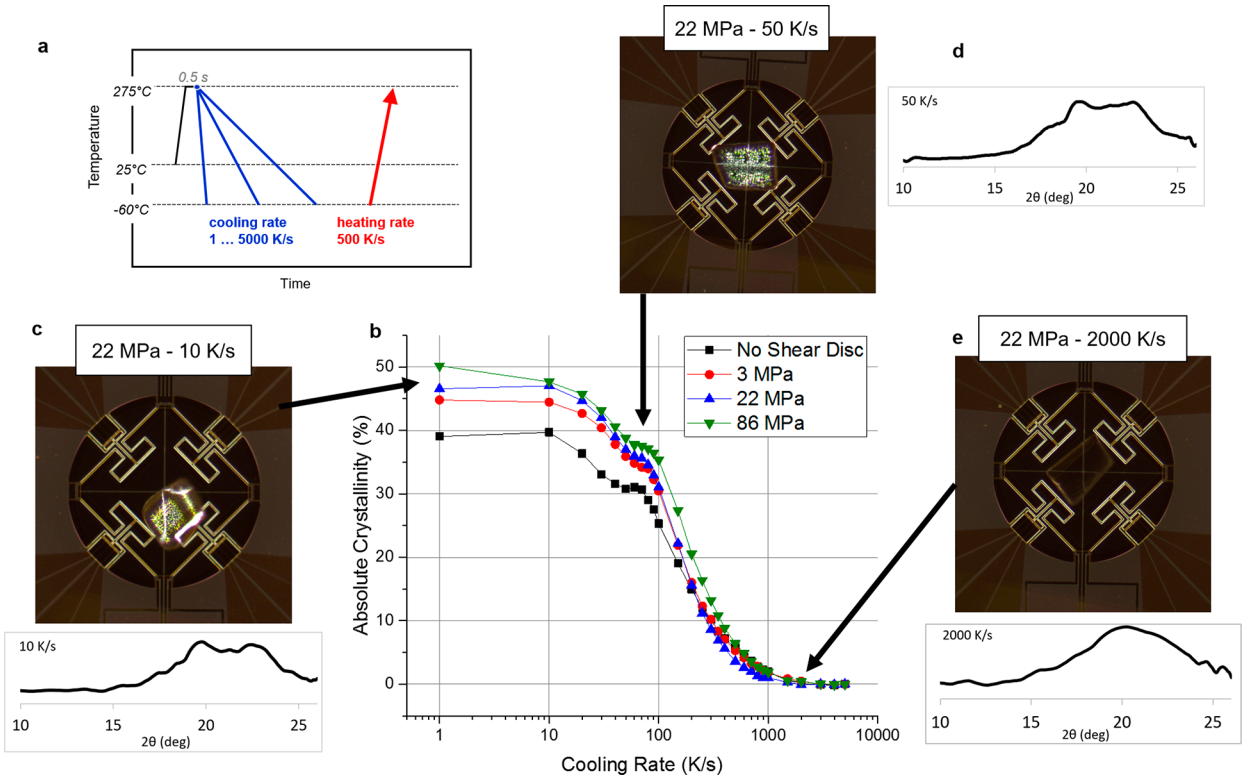

Figure 5. Critical cooling rate and absolute crystalline content evaluation. (a) Each shish-containing sample was subject to the method shown. Note that the melt was subject to 275 °C, which is below the equilibrium melting temperature. (b) depicts the resulting crystallinity formed upon cooling at the indicated rate. The data indicate that the absolute crystalline content increases with higher amounts of shear work prior to crystallization. (c, d, and e) are examples of the PA 66 analyzed via both POM and WAXS immediately after being subject to the indicated cooling rate.

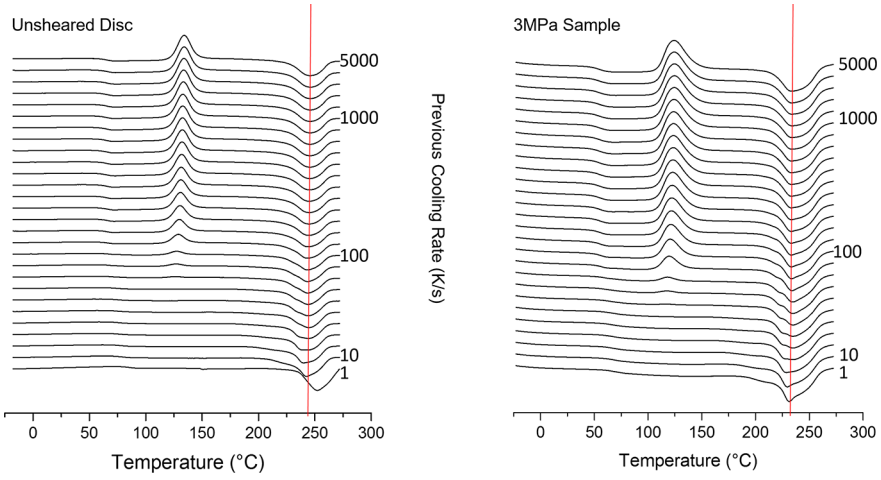

Figure 6. Subsequent heating curves, obtained at 500 K/s after the sample was subject to the indicated cooling rate.

temperature is 140 °C while the 86 MPa sample transition temperature is 125 °C, indicating that the formation of the stable α-phase is likely feasible at lower temperatures than are possible in the unsheared sample.

3.2. Nonisothermal Crystallization and Critical Cooling Rates. Next samples were equilibrated at 275 °C and then cooled at the rate of 1 K/s to −60 °C. Immediately after cooling, the sample was remelted by heating at a rate of 500 K/s to 275 °C. After data collection, the method was repeated on the same sample, systematically increasing the cooling rate from 1 to 5000 K/s (Figure 5a). The cooling scans revealed the temperature and enthalpy of crystallization, while the subsequent heating scans were used to determine the fraction of crystals formed during cooling by considering both cold-crystallization and melting enthalpies.

The absolute amount of crystalline content formed during cooling of the PA 66 melt is a function of both the cooling rate and the level of shear work previously experienced by the sample. At slow cooling rates, shear-induced precursors actively nucleate the crystallization process and result in a detectable increase in crystalline content with increasing shear work; the nonsheared PA 66 results in approximately 20% less crystalline content than the highly sheared counterpart. As the cooling rate is increased to 100 K/s, the sheared samples consistently

DOI: 10.1021/acs.macromol.8b00195
Macromolecules XXXX, XXX, XXX−XXX

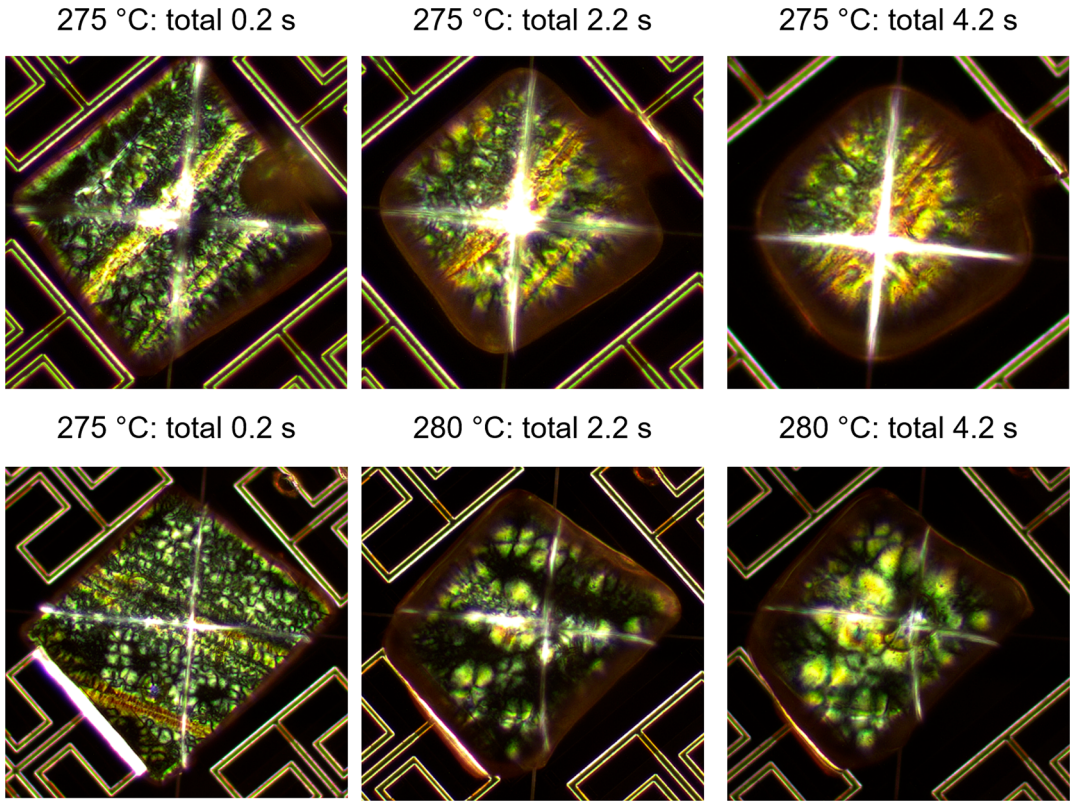

Figure 7. Optical and calorimetric evidence of flow-induced structure lifetime. PA 66 (22 MPa sample) shish-kebab structures on FSC sensor as cut and then after each condition indicated (maximum 275 °C top row, 280 °C bottom row).

develop more crystalline content, the magnitude of which tracks with the prior shear work loading. Wide-angle X-ray analysis of the samples on the FSC sensor indicates the α-crystalline phase has developed after cooling at 10 and 50 K/s (Figure 5c,d). As cooling rates approach 200 K/s, however, we observe an interesting phenomenon. The 3 and 22 MPa samples suddenly begin to track with the unsheared sample, all three of which result in an absolute crystallinity of 15%. At this rate, the shear-induced structures present in the 86 MPa sample are still able to nucleate crystallization and result in a slightly higher 21% absolute crystallinity. Above 200 K/s all samples produce about the same amount of crystallinity upon cooling, and if cooling at rates higher than 1000 K/s, then PA 66 is vitrified to the amorphous glass (Figure 5e).

Examination of the heating curves obtained after each cooling rate experiment reveals a difference in the shape of the melting peaks for the 3 MPa sheared and the unsheared PA 66, likely indicating a more complex microstructure population in the sheared sample. Each sheared sample displays an asymmetric melting peak with a broader, lower peak melting temperature of approximately 231 °C, notably lower than the typical peak melting temperature of 248 °C observed in the unsheared sample. While the onset of cold crystallization upon heating begins after approximately the same cooling conditions for both the sheared and unsheared sample, the magnitude of cold crystallization is greater in the sheared sample. This indicates that the flow-induced precursors also nucleate cold crystallization. This is particularly evident in the cold-crystallization behavior after cooling at 100 K/s.

3.3. FIC Nucleating Structure Survival at $T_m > T_m^0$. At $T > T_m^0$, any structures formed during FIC should be destroyed and melt memory erased. For PA 66, T_m^0 has been experimentally determined at 277.4 °C, using the linear Hoffman–Weeks approach.[46] The HW approach is experimentally simple; the linear regression of experimentally observed T_m for samples crystallized at specific temperature (T_c) is extended to the equilibrium line, where $T_c = T_m$. The HW approach assumes that lamellar thickening at a given T_c is responsible for the subsequent observable T_m, and in some cases it has been shown to fail for polymers crystallized at very low undercoolings.[62] While a more robust calculation of T_m^0 is possible with additional experimental rigor, T_m^0 as calculated here (277.4 °C) provides an estimate that proves useful.[63] Samples heated to temperatures less than T_m^0 do not lose their flow-induced crystallization behavior with repeated cycles, while the samples heated to $T_m > T_m^0$ lose their flow-induced crystallization behavior with time. To study the survival of FIC structures at $T > T_m^0$, we employ both POM and FSC in an effort to differentiate the presence of visible shish structures from the potential nucleating influence of flow-induced precursors that may persist in the melt after the dissolution of the chain-extended shish crystal. Practical implications abound, as polymer engineers are challenged to erase the *thermal history* of a melt prior to advanced characterization or manufacturing techniques. Adopting the same sample preparation techniques, the lifetime of shish at a specific temperature in the melt was studied on the FSC sensor, where the sample was subject to a series of very short (1 s) holds in the melt followed by an isothermal melt-crystallization step at 200 °C, a temperature known to induce growth of large spherulitic structures.[56] Between each isothermal step, the sample was quenched at 2000 K/s, and the FSC sensor chip was taken out of the calorimeter to analyze the evolved structure through POM.

DOI: 10.1021/acs.macromol.8b00195
Macromolecules XXXX, XXX, XXX–XXX

Care was taken to ensure at least one shish structure was clearly visible in the FSC sample prior to running each experiment. First, each sample was heated at 500 K/s to 275 °C for 0.2 s, then quenched at 2000 K/s to 200 °C, and allowed to crystallize. The sample was then heated to the target annealing temperature for 1 s and then quenched at 2000 K/s to the target isothermal crystallization temperature of 200 °C, and the crystallization isotherm was collected. The material was quenched back to −60 °C, and the cycle was repeated 20 times. The final isotherm collected for each sample represents crystallization after a cumulative 20 s in the melt.

Between isothermal crystallization steps, the sensor containing the PA 66 sample was examined under POM. In Figure 7a, we show the samples on the FSC chips for both the study at 275 °C and the study at 280 °C. Initially, both samples contain visible shish-kebab structures. After 4 s in the melt at 275 °C the shish structures remain, though the sample begins to form a droplet shape, indicative of melt relaxation. While chain relaxation is evident in portions of the melt, chains that comprise the flow-induced precursors remain associated in the melt.[64] Meanwhile, there is a visible loss of oriented structure that occurs after 2.2 s above the equilibrium melting temperature of 277 °C, and after 4.2 s oriented structures appear to be destroyed. However, the loss of visible structure does not equate to a loss of nucleating function in the melt.

The isothermal crystallization traces for the 22 MPa sample aged at 275 °C (Figure 8a) indicate that the peak time of crystallization is constant at 0.24 s even after 20 s in melt at 275 °C, a logical result in accord with the POM discussed above. In contrast, the accelerating influence of the nucleating structures formed under shear began to diminish after 2 s in the melt at a temperature of 280 °C, paralleling the loss of orientation in POM. Here more time is required to reach the peak of crystallization at 200 °C (Figure 8b), indicating a loss of nucleating efficiency driven by the destruction of shear-induced structures at the equilibrium melting temperature. However, the loss in efficiency is not complete after 4 s as expected from POM. With each successive stay in the melt at 280 °C the peak time of crystallization increases slightly until, after a cumulative time of 20 s in the melt at 280 °C, the peak time of crystallization increases to that of the zero-shear PA 66, approximately 0.5 s.

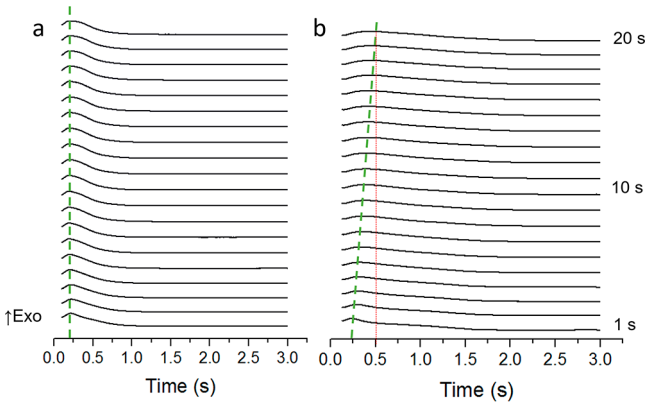

Figure 8. (a) Isothermal crystallization curves collected for the PA 66 (22 MPa disc) at 200 °C from the same sample, after being held in the melt at 275 °C for the indicated time. Notice the peak isothermal crystallization time does not change after 20 s in the melt at 275 °C. (b) Isothermal crystallization curves collected for the PA 66 (22 MPa) at 200 °C from the same sample, after being held in the melt at 285 °C for the indicated time. For reference, the no-shear sample peak time is 0.5 s at 200 °C, indicated by the red dotted line.

4. CONCLUSIONS

This study details the first experimental approach to quantify the influence of specific amounts of shear work on polymer crystallization across all levels of supercooling. The concept that specific shear work in the melt results in accelerated crystallization at low supercooling has already been shown for iPP and other polymers.[36,39,41,65] The unsheared crystallization behavior of PA 66 is also qualitatively similar to several other polymers.[10] Therefore, it is logical to expect that most other polymers will display the shear-induced work sensitivity across the entire heterogeneous nucleation temperature range.

While FSC is an established tool for the investigation of quiescent polymer crystallization, we are the first to apply it to flow-induced crystallization, the important mechanism induced by nearly all forms of polymer processing. Because the sample size for FSC is sufficiently small, shish-kebab structures created under very exact, known shearing conditions in the melt have been isolated for FSC analysis, and their influence on subsequent crystallization processes was determined at both low and high supercooling. This study reveals that the polymer crystallization process is remarkably sensitive to the amount of shear experienced in the melt across all temperatures where the heterogeneous nucleation mechanism dominates crystalline growth (T_c > 135 °C for PA 66) and that the sheared samples are able to crystallize via the heterogeneous nucleation route 15 K below thermal limit of the unsheared materials. Many polymer manufacturing processes such as injection molding rapid cooling push solidification into this low-temperature regime, and so extending the α-polymorph development to lower temperatures is relevant. In the lowest temperature regime, the presence of flow-induced precursors has no influence on homogeneous nucleation-driven crystallization. The magnitude of previous shear flow drives crystalline conversion rate, α-/γ- crystalline phase development, and crystallization during cooling. Precursor lifetime, as observed by accelerated crystallization, is very long at 275 °C (below the T_m^0) but is quite short at 280 °C (above T_m^0). We have also discovered that the nucleating influence of shear-induced structures is not limited to shish visible in POM but that the accelerating influence persists up to 15 s after visible shish disappear at a critical temperature near the calculated T_m^0.

We expect that the crystallization behavior here is not unique to PA 66 and that this technique is useful to develop important thermodynamic and kinetic insights to describe the crystallization behavior of many important polymers and polymeric systems. Increasingly, polymer applications demand attributes such as controlled degradation, predictable phase separation, and microscale feature development. In the future, the development of precise and predictable microstructure during manufacturing will require results such as those exemplified in this study to improve and inform crystallization models. For instance, we discovered that shear does nothing to the imperfect γ-phase that form at temperatures near T_g, but shear provides a strong acceleration of the desirable α-crystals, effectively tipping the balance to favor these crystals, which are known to result in better mechanical properties after injection molding. These specific results can be used to design an optimized melt-flow process for PA 66 that includes control over flow strength, time in the melt, and cooling conditions in

DOI: 10.1021/acs.macromol.8b00195
Macromolecules XXXX, XXX, XXX−XXX

order to produce such intentional microstructure during manufacturing. Generalizing this concept to develop a broad, new approach for the design of polymer manufacturing processes will require comprehensive studies that investigate microstructure development and stability at all levels of supercooling, and this study provides a template for such future work.

AUTHOR INFORMATION

Corresponding Author

*(A.M.R.) E-mail amh234@psu.edu; Tel +1-814-898-6287.

ORCID

Alicyn M. Rhoades: 0000-0003-4678-419X

René Androsch: 0000-0002-7924-0159

Ralph H. Colby: 0000-0002-5492-6189

Funding

This material is based upon work supported by the National Science Foundation under Grant CMMI-1653629 and the Deutsche Forschungsgemeinschaft (DFG) (Grant AN 212/20-2).

Notes

The authors declare no competing financial interest.

ACKNOWLEDGMENTS

The authors thank Nichole Wonderling of the Penn State University Materials Characterization Laboratories for assistance with wide-angle X-ray measurements and Hideaki Takahashi of the Toray Research Center, Inc., for molecular weight characterization.

REFERENCES

(1) Housmans, J.-W.; Peters, G. W. M.; Meijer, H. E. H. Flow-Induced Crystallization of Propylene/Ethylene Random Copolymers. *J. Therm. Anal. Calorim.* **2009**, *98*, 693−705.

(2) Zheng, R.; Kennedy, P. K. A Model for Post-Flow Induced Crystallization: General Equations and Predictions. *J. Rheol.* **2004**, *48*, 823−842.

(3) Sorrentino, A.; De Santis, F.; Titomanlio, G. Polymer Crystallization under High Cooling Rate and Pressure: A Step Towards Polymer Processing Conditions. *Lect. Notes Phys.* **2007**, *714*, 329−344.

(4) Janeschitz-Kriegl, H. How to Understand Nucleation in Crystallizing Polymer Melts under Real Processing Conditions. *Colloid Polym. Sci.* **2003**, *281*, 1157−1171.

(5) Lamberti, G. Flow Induced Crystallization of Polymers. *Chem. Soc. Rev.* **2014**, *43*, 2240−2252.

(6) Jariyavidyanont, K.; Williams, J. L.; Rhoades, A. M.; Kühnert, I.; Focke, W.; Androsch, R. Crystallization of Polyamide 11 During Injection Molding. *Polym. Eng. Sci.* **2017**, DOI: 10.1002/pen.24665.

(7) Kim, K.; Isayev, A. I.; Kwon, K. Flow-Induced Crystallization in the Injection Molding of Polymers: A Thermodynamic Approach. *J. Appl. Polym. Sci.* **2005**, *95*, 502−523.

(8) Janeschitz-Kriegl, H. *Crystallization Modalities in Polymer Melt Processing: Fundamental Aspects of Structure Formation*; Springer: New York, 2012.

(9) Androsch, R.; Toda, A.; Schick, C. Insights into Polymer Crystallization and Melting from Fast Scanning Chip Calorimetry. *Polymer* **2016**, *91*, 239−263.

(10) Androsch, R.; Schick, C. Crystal Nucleation of Polymers at High Supercooling of the Melt. *Adv. Polym. Sci.* **2015**, *276*, 257−288.

(11) Silvestre, C.; Cimmino, S.; Duraccio, D.; Schick, C. Isothermal Crystallization of Isotactic Poly(Propylene) Studied by Superfast Calorimetry. *Macromol. Rapid Commun.* **2007**, *28*, 875−881.

(12) Rhoades, A. M.; Wonderling, N.; Gohn, A.; Williams, J.; Mileva, D.; Gahleitner, M.; Androsch, R. Effect of Cooling Rate on Crystal Polymorphism in Beta-Nucleated Isotactic Polypropylene as Revealed by a Combined Waxs/Fsc Analysis. *Polymer* **2016**, *90*, 67−75.

(13) Wurm, A.; Herrmann, A.; Cornelius, M.; Zhuravlev, E.; Pospiech, D.; Nicula, R.; Schick, C. Temperature Dependency of Nucleation Efficiency of Carbon Nanotubes in Pet and Pbt. *Macromol. Mater. Eng.* **2015**, *300*, 637−649.

(14) Schick, C.; Androsch, R.; Schmelzer, J. Homogeneous Crystal Nucleation in Polymers. *J. Phys.: Condens. Matter* **2017**, *29*, 453002.

(15) Rhoades, A. M.; Wonderling, N.; Schick, C.; Androsch, R. Supercooling-Controlled Heterogeneous and Homogenous Crystal Nucleation of Polyamide 11 and Its Effect onto the Crystal/Mesophase Polymorphism. *Polymer* **2016**, *106*, 29−34.

(16) Androsch, R.; Rhoades, A. M.; Stolte, I.; Schick, C. Density of Heterogeneous and Homogeneous Crystal Nuclei in Poly (Butylene Terephthalate). *Eur. Polym. J.* **2015**, *66*, 180−189.

(17) Androsch, R.; Schick, C.; Schmelzer, J. W. Sequence of Enthalpy Relaxation, Homogeneous Crystal Nucleation and Crystal Growth in Glassy Polyamide 6. *Eur. Polym. J.* **2014**, *53*, 100−108.

(18) Zhuravlev, E.; Schmelzer, J. W.; Wunderlich, B.; Schick, C. Kinetics of Nucleation and Crystallization in Poly (ε-Caprolactone)-(Pcl). *Polymer* **2011**, *52*, 1983−1997.

(19) Di Lorenzo, M. L. The Crystallization and Melting Processes of Poly(L-Lactic Acid). *Macromol. Symp.* **2006**, *234*, 176−183.

(20) Peters, G. M. W.; Balzano, L.; Steenbakkers, R. J. A. Flow-Induced Crystallization. In *Handbook of Polymer Crystallization*; John Wiley & Sons, Inc.: Hoboken, NJ, 2013; pp 399−432.

(21) Acierno, S.; Palomba, B.; Winter, H. H.; Grizzuti, N. Effect of Molecular Weight on the Flow-Induced Crystallization of Isotactic Poly(1-Butene). *Rheol. Acta* **2003**, *42*, 243−250.

(22) Wingstrand, S. L.; Shen, B.; Kornfield, J. A.; Mortensen, K.; Parisi, D.; Vlassopoulos, D.; Hassager, O. Rheological Link between Polymer Melts with a High Molecular Weight Tail and Enhanced Formation of Shish-Kebabs. *ACS Macro Lett.* **2017**, *6*, 1268−1273.

(23) Wang, Z.; Ma, Z.; Li, L. Flow-Induced Crystallization of Polymers: Molecular and Thermodynamic Considerations. *Macromolecules* **2016**, *49*, 1505−1517.

(24) Flory, P. J. Thermodynamics of Crystallization on High Polymers. I. Crystallization Induced by Stretching. *J. Chem. Phys.* **1947**, *15*, 397−408.

(25) Kornfield, J. A.; Kumaraswamy, G.; Issaian, A. M. Recent Advances in Understanding Flow Effects on Polymer Crystallization. *Ind. Eng. Chem. Res.* **2002**, *41*, 6383−6392.

(26) Kimata, S.; Sakurai, T.; Nozue, Y.; Kasahara, T.; Yamaguchi, N.; Karino, T.; Shibayama, M.; Kornfield, J. Molecular Basis of the Shish-Kebab Morphology in Polymer Crystallization. *Science* **2007**, *316*, 1014−1017.

(27) Kumaraswamy, G.; Issaian, A. M.; Kornfield, J. A. Shear-Enhanced Crystallization in Isotactic Polypropylene. 1. Correspondence between in-Situ Rheo-Optics and Ex-Situ Structure Determination. *Macromolecules* **1999**, *32*, 7537−7547.

(28) Shen, B.; Liang, Y.; Kornfield, J. A.; Han, C. C. Mechanism for Shish Formation under Shear Flow: An Interpretation from an in Situ Morphological Study. *Macromolecules* **2013**, *46*, 1528−1542.

(29) Cui, K.; Ma, Z.; Tian, N.; Su, F.; Liu, D.; Li, L. Multiscale and Multistep Ordering of Flow-Induced Nucleation of Polymers. *Chem. Rev.* **2018**, *118*, 1840−1886.

(30) Balzano, L.; Ma, Z.; Cavallo, D.; van Erp, T. B.; Fernandez-Ballester, L.; Peters, G. W. M. Molecular Aspects of the Formation of Shish-Kebab in Isotactic Polypropylene. *Macromolecules* **2016**, *49*, 3799−3809.

(31) Liu, D.; Tian, N.; Huang, N.; Cui, K.; Wang, Z.; Hu, T.; Yang, H.; Li, X.; Li, L. Extension-Induced Nucleation under near-Equilibrium Conditions: The Mechanism on the Transition from Point Nucleus to Shish. *Macromolecules* **2014**, *47*, 6813−6823.

(32) Hamad, F.; Colby, R.; Milner, S. Lifetime of Flow-Induced Precursors in Isotactic Polypropylene. *Macromolecules* **2015**, *48*, 7286−7299.

(33) Binsbergen, F. Orientation-Induced Nucleation in Polymer Crystallization. *Nature* **1966**, *211*, 516−517.

DOI: 10.1021/acs.macromol.8b00195
Macromolecules XXXX, XXX, XXX−XXX

(34) Janeschitz-Kriegl, H.; Eder, G. Shear Induced Crystallization, a Relaxation Phenomenon in Polymer Melts: A Re-Collection. *J. Macromol. Sci., Part B: Phys.* **2007**, *46*, 591−601.
(35) Hayashi, Y.; Matsuba, G.; Zhao, Y.; Nishida, K.; Kanaya, T. Precursor of Shish−Kebab in Isotactic Polystyrene under Shear Flow. *Polymer* **2009**, *50*, 2095−2103.
(36) Housmans, J. W.; Steenbakkers, R. J. A.; Roozemond, P. C.; Peters, G. W.; Meijer, H. E. H. Saturation of Pointlike Nuclei and Transition to Oriented Structures in Flow-Induced Crystallization of Isotactic Polypropylene. *Macromolecules* **2009**, *42*, 5728−5740.
(37) Okura, M.; Chambon, P.; Mykhaylyk, O. O.; Fairclough, J. P. A.; Ryan, A. J. Using Multimodal Blends to Elucidate the Mechanism of Flow-Induced Crystallization in Polymers. *J. Polym. Sci., Part B: Polym. Phys.* **2011**, *49*, 621−628.
(38) Janeschitz-Kriegl, H.; Ratajski, E.; Stadlbauer, M. Flow as an Effective Promotor of Nucleation in Polymer Melts: A Quantitative Evaluation. *Rheol. Acta* **2003**, *42*, 355−364.
(39) Mykhaylyk, O. O; Chambon, P.; Graham, R. S.; Fairclough, J. P. A.; Olmsted, P. D.; Ryan, A. J. The Specific Work of Flow as a Criterion for Orientation in Polymer Crystallization. *Macromolecules* **2008**, *41*, 1901−1904.
(40) Hamad, F.; Colby, R.; Milner, S. Onset of Flow-Induced Crystallization Kinetics of Highly Isotactic Polypropylene. *Macromolecules* **2015**, *48*, 3725−3738.
(41) Nazari, B.; Rhoades, A. M.; Schaake, R. P.; Colby, R. H. Flow-Induced Crystallization of Peek: Isothermal Crystallization Kinetics and Lifetime of Flow-Induced Precursors During Isothermal Annealing. *ACS Macro Lett.* **2016**, *5*, 849.
(42) Hamad, F. G.; Colby, R. H.; Milner, S. T. Transition in Crystal Morphology for Flow-Induced Crystallization of Isotactic Polypropylene. *Macromolecules* **2016**, *49*, 5561−5575.
(43) Jerschow, P.; Janeschitz-Kriegl, H. The Role of Long Molecules and Nucleating Agents in Shear Induced Crystallization of Isotactic Polypropylenes. *Int. Polym. Process.* **1997**, *12*, 72−77.
(44) Nogales, A.; Hsiao, B. S.; Somani, R. H.; Srinivas, S.; Tsou, A. H.; Balta-Calleja, F. J.; Ezquerra, T. A. Shear-Induced Crystallization of Isotactic Polypropylene with Different Molecular Weight Distributions: In Situ Small- and Wide-Angle X-Ray Scattering Studies. *Polymer* **2001**, *42*, 5247−5256.
(45) Zytel Molding Guide 1995; http://plastics.dupont.com/plastics/pdflit/americas/zytel/198118E.pdf.
(46) Hoffman, J.; Weeks, J. Melting Process and the Equilibrium Melting Temperature of Polychlorotrifluoroethylene. *J. Res. Natl. Bur. Stand., Sect. A* **1962**, *66*, 13−28.
(47) Mourey, T. H.; Bryan, T. G. Size-Exclusion Chromatography in 1,1,1,3,3,3,-Hexafluoro-2-Propanol. *J. Chromatogr. A* **2002**, *964*, 169−178.
(48) Zhou, W.-J.; Kornfield, J. A.; Ugaz, V. M.; Burghardt, W. R.; Link, D. R.; Clark, N. A. Dynamics and Shear Orientation Behavior of a Main-Chain Thermotropic Liquid Crystalline Polymer. *Macromolecules* **1999**, *32*, 5581−5593.
(49) Fernandez-Blazquez, J. P.; Bello, A.; Perez, E. Parallel and Perpendicular Orientation in a Thermotropic Main-Chain Liquid-Crystalline Polymer. *Macromolecules* **2007**, *40*, 703−709.
(50) Hu, W.; Frenkel, D.; Mathot, V. B. F. Simulation of Shish-Kebab Crystallite Induced by a Single Prealigned Macromolecule. *Macromolecules* **2002**, *35*, 7172−7174.
(51) Romo-Uribe, A.; Windle, A. H. "Log-Rolling" Alignment in Main-Chain Thermotropic Liquid Crystalline Polymer Melts under Shear: An in-Situ Waxs Study. *Macromolecules* **1996**, *29*, 6246−6255.
(52) Mathot, V.; Pyda, M.; Pijpers, T.; Vanden Poel, G.; van de Kerkhof, E.; van Herwaarden, S.; van Herwaarden, A.; Leenaers, A. The Flash Dsc 1, a Power Compensation Twin-Type, Chip-Based Fast Scanning Calorimeter (Fsc): First Findings on Polymers. *Thermochim. Acta* **2011**, *522*, 36−45.
(53) van Herwaarden, S.; Iervolino, E.; van Herwaarden, F.; Wijffels, T.; Leenaers, A.; Mathot, V. Design, Performance and Analysis of Thermal Lag of the Ufs1 Twin Calorimeter Chip for Fast Scanning Calorimetry Using the Mettler-Toldeo Flash Dsc 1. *Thermochim. Acta* **2011**, *522*, 46−52.
(54) Iervolino, E.; van Herwaarden, A. W.; van de Kerkhof, P.; van Grinsven, A.; Leenaers, A.; Mathot, V.; Sarro, P. Temperature Calibration and Electrical Characterization of the Differential Scanning Calorimeter Chip Ufs1 for the Mettler Toledo Flash Dsc 1. *Thermochim. Acta* **2011**, *522*, 53−59.
(55) Monnier, X.; Chevalier, L.; Esposito, A.; Fernandez-Ballester, L.; Saiter, A.; Dargent, E. Local and Segmental Motions of the Mobile Amorphous Fraction in Semi-Crystalline Polylactide Crystallized under Quiescent and Flow-Induced Conditions. *Polymer* **2017**, *126*, 141−151.
(56) Gohn, A.; Rhoades, A. M.; Wonderling, N.; Tighe, T.; Androsch, R. The Effect of Supercooling of the Melt on the Semicrystalline Morphology of Pa 66. *Thermochim. Acta* **2017**, *655*, 313−318.
(57) Schawe, J. E. K.; Pötschke, P.; Alig, I. Nuclation Efficiency of Fillers in Polymer Crystallization Studied by Fast Scanning Calorimetry; Carbon Nanotubes in Polypropylene. *Polymer* **2017**, *116*, 160−172.
(58) Androsch, R.; Monami, A.; Kucera, J. Effect of an Alpha-Phase Nucleating Agent on the Crystallization Kinetics of a Propylene/Ethylene Randome Copolymer at Largely Different Supercooling. *J. Cryst. Growth* **2014**, *408*, 91−96.
(59) Mollova, A.; Androsch, R.; Mileva, D.; Gahleitner, M.; Funari, S. S. Crystallization of Isotactic Polyporpylene Containing Beta-Phase Nucleating Aget at Rapid Cooling. *Eur. Polym. J.* **2013**, *49*, 1057−1065.
(60) Kolesov, I.; Androsch, R.; Mileva, D.; Lebek, W.; Benhamida, A.; Kaci, M.; Focke, W. Crystallization of a Polyamide 11/Organo-Modified Montmorillonite Nanocomposite at Rapid Cooling. *Colloid Polym. Sci.* **2013**, *291*, 2541−2549.
(61) Schawe, J. E.; Vermeulen, P. A.; van Drongelen, M. A New Crystallization Process in Polypropylene Highly Filled with Calcium Carbonate. *Colloid Polym. Sci.* **2015**, *293*, 1607−1614.
(62) Alamo, R. G.; Viers, B. D.; Mandelkern, L. A Re-Examinatino of the Relation between the Melting Temperature and the Crystallization Temperture: Linear Polyethylene. *Macromolecules* **1995**, *28*, 3205−3213.
(63) Marand, H.; Xu, J.; Srinivas, S. Determinatin of the Equilibrium Melting Temperature of Polymer Crystals: Linear and Nonlinear Hoffman-Weeks Extrapolations. *Macromolecules* **1998**, *31*, 8219−8229.
(64) Shen, B.; Liang, Y.; Kornfield, J.; Han, C. Mechanism for Shish Formation under Shear Flow: An Interpretation from an in Situ Morphological Study. *Macromolecules* **2013**, *46*, 1528−1542.
(65) Housmans, J.-W.; Peters, G. W. M.; Meijer, H. E. H. Flow-Induced Crystallization of Propylene/Ethylene Random Copolymers. *J. Therm. Anal. Calorim.* **2009**, *98*, 693−705.

DOI: 10.1021/acs.macromol.8b00195
Macromolecules XXXX, XXX, XXX−XXX